**Proceedings of ASME Turbo Expo 2011**
**GT2011**
**June 6-10, 2011, Vancouver, British Columbia, Canada**

**GT2011-46705**

# AN IMPROVED CORE REACTION MECHANISM FOR SATURATED $C_0$-$C_4$ FUELS

**Chitralkumar V. Naik***
Reaction Design
San Diego, California, USA

**Karthik V. Puduppakkam**
Reaction Design
San Diego, California, USA

**Ellen Meeks**
Reaction Design
San Diego, California, USA

## ABSTRACT

Accurate chemistry models are required to predict the combustion behavior of different fuels, such as synthetic gaseous fuels and liquid jet fuels. A detailed reaction mechanism contains chemistry for all the molecular components in the fuel or its surrogates. Validation studies that compare model predictions with the data from fundamental combustion experiments under well defined conditions. Such fundamental experiments are least affected by the effect of transport on chemistry. Therefore they are the most reliable means for determining a reaction mechanism's predictive capabilities. Following extensive validation studies and analysis of detailed reaction mechanisms for a wide range of hydrocarbon components reported in our previously published work [1-5], we identified some common issues in the predictive nature of the mechanisms that are associated with inadequacies of the core ($C_0$-$C_4$) mechanism. For example predictions of laminar flame speeds and autoignition delay times for several fuels were inaccurate beyond the level of uncertainty in the data. This core mechanism is shared by all of the mechanisms for the larger hydrocarbon components. Unlike the reaction paths for larger hydrocarbon fuels, however, reaction paths for the core chemistry do not follow prescribed reaction rate-rules. In this work, we revisit our core reaction mechanism for saturated $C_0$-$C_4$ fuels, with the goal of improving predictions for the widest range of fundamental experiments as possible. To evaluate and validate the mechanism improvements, we performed a broad set of simulations of fundamental experiments. These experiments include measurements of ignition delay, flame speed and extinction strain rate, as well as species composition in stirred reactors, flames and flow reactors. The range of conditions covers low to high temperatures, very lean to very rich fuel-air ratios, and low to high pressures. Our core reaction mechanism contains thermochemical parameters derived from a wide variety of sources, including experimental measurements, ab initio calculations, estimation methods and systematic optimization studies. Each technique has its uncertainties and potential inaccuracies. Using a systematic approach that includes sensitivity analysis, reaction-path analysis, consideration of recent literature studies, and an attention to data consistency, we have identified key updates required for the core mechanism. These updates resulted in accurate predictions for various saturated fuels when compared to the data over a broad range of conditions. All reaction rate constants and species thermodynamics and transport parameters remain within known uncertainties and within physically reasonable bounds. Unlike most mechanisms in the literature, the mechanism developed in this work is self-consistent and contains chemistry of all saturated $C_0$-$C_4$ fuels.

## 1. INTRODUCTION

Core chemistry involving species from $C_0$ (or $H_2$) to $C_4$ is very important for modeling combustion characteristics of natural gas and other gaseous fuels. It also forms the base of the larger liquid fuel mechanisms that are used to represent surrogate gasoline, diesel, jet and biomass-derived fuels. Therefore, an accurate core mechanism is extremely important for predicting combustion characteristics of all gaseous and liquid fuels, including accurate predictions of $NO_x$ and precursors of poly-aromatic hydrocarbons (PAH) that lead to soot formation.

All detailed reaction mechanisms in the literature for natural gas and liquid fuels contain the core chemistry of $C_0$ to $C_4$ hydrocarbons. However, many mechanisms have not been validated for smaller hydrocarbons and may not be comprehensive and accurate enough to be used for all saturated gaseous fuel components [6-9]. On the other hand, many available detailed reaction mechanisms for smaller hydrocarbons are not sufficiently comprehensive to represent all saturated core components [10-13] (such as GRI-mech 3.0 [14]). Merging mechanisms developed separately for various fuels results in inconsistencies in the mechanism. Such mechanism is very likely

to yield predictions that are different and inaccurate than their source mechanisms. The goal of this work is to develop an accurate and self-consistent detailed reaction mechanism consisting chemistry for all saturated hydrocarbons and several important oxygenated hydrocarbons in the $C_0$ to $C_4$ range, and then validate the mechanism over a broad range of conditions using diverse fundamental experimental data that are available in the literature. In this work we have focused on eleven (11) fuel components, including hydrogen, CO, methane, ethane, propane, *n*-butane, *iso*-butane, methanol, ethanol, dimethyl ether (DME) and *n*-butanol. This work is the first in a pair of publications on comprehensive and accurate core reaction-mechanism work. In the upcoming publication, we will focus on the improved mechanism for unsaturated hydrocarbons and various fuel blends [15].

## 2. MECHANISM DEVELOPMENT

The "original or initial reference" core mechanism is the core component of several mechanisms reported previously for different liquid-fuel studies [1-5]. Many of the reaction paths and reaction rate constants in the original core mechanism are common to those of the core component of liquid-fuels mechanisms published by Pitz et al. [7, 9, 16] and Naik et al. [8, 17]. Predictions using this initial reference mechanism were inaccurate for several conditions and fuels. For example, laminar flame speeds for some of the saturated and unsaturated fuels were overpredicted. Predicted trends in autoignition delay times were also inaccurate for fuel blends and for some of the unsaturated fuels. In the mechanism development work, we more closely examined all reaction systems that are important for combustion of various fuels, starting from hydrogen and building the mechanisms for larger fuels up to $C_4$ in a stepwise fashion. At each step, then, we were building on an established, validated set of core kinetics. The improved core mechanism is referred to as the Reaction Design 2010 mechanism or the "RD2010" mechanism. This mechanism also includes the detailed kinetics of unsaturated hydrocarbons, such that the mechanism contains carbon species up to $C_6$ and their elementary reactions. These reactions include the chemistry for forming the first benzene ring, which is crucial for polycyclic aromatic hydrocarbons (PAH) growth. The detailed mechanism consists of 1161 species and 5622 elementary reaction steps. In this article, we provide an overview of the methodology used in improving the original mechanism and then present extensive validation of the resulting RD2010 mechanism.

Several researchers, including Konnov et al. [18], Li et al. [11] and O'Conaire et al. [19] have studied $H_2$ oxidation chemistry. We based our $H_2$ mechanism primarily on the recent work of Konnov et al., with some rate coefficients taken from other published studies [11, 19, 20]. A comprehensive description of chemistry, including reactions involved in oxidation of CO, methane ($CH_4$), formaldehyde ($CH_2O$), and methanol ($CH_3OH$), was included in the $C_1$ subset of the mechanism. Many reaction-rate coefficients were collected based on recent mechanisms from Healy et al. [12], Li et al. [11] and Sirjean et al. [13]. Similarly, a comprehensive set of reactions for ethane ($C_2H_6$), ethylene ($C_2H_4$), acetylene ($C_2H_2$), ethanol ($C_2H_5OH$), and acetaldehyde ($CH_3CHO$) were included in the $C_2$ submechanism. In addition, we also added the reactions pertaining to dimethyl ether (DME, $CH_3OCH_3$) oxidation from Healy et al. [12] to form a comprehensive base mechanism. Additional reactions from the mechanisms by Laskin et al. [21] and Zhang et al. [22] were also added to the mechanism. These reactions involve species such as $C_2H$, $C_2O$, $C_2$, etc., that are important for fuel-rich and high-temperature conditions and for PAH precursor chemistry. Similarly, we also updated most hydrogen abstraction reactions based on recent publications [12]. All important unimolecular dissociations of stable species and radicals have been assigned pressure-dependent rate coefficients using the Troe formulation [23].

Rate-parameter uncertainty was considered for several important reactions, based on the collection of values for rate constants reported in the NIST Chemical Kinetics database [24] as well as those used in various published mechanisms. In addition to experimental uncertainties in measured rate constants, we also considered the scatter in rate-constants data from different sources, which indicates uncertainties associated with kinetic estimations. The mechanism was first assembled to be as complete as scientifically necessary for combustion modeling using unadjusted rate constants assigned to all elementary reactions. Then, based on the level of uncertainty, several rate constants were adjusted within the uncertainty range to optimize prediction accuracy over a broad range of conditions. The typical level of uncertainty in rate constants varies from 20% for dominant and well-studied reactions to a factor of 2 for most other reactions. Rate constants were adjusted only for a handful of reactions (less than 5% of the total number of reactions) in the mechanism, relative to original sources. Many types of fundamental experiments were considered for validation, as presented in the next section and in the future publication on unsaturated components and fuel blends [15]. Important reactions were identified based on flux and sensitivity analysis for validation cases and selected cases covering broad range of conditions are presented in the next section.

In addition to the hydrocarbon combustion chemistry, detailed $NO_x$-formation and fuel-$NO_x$ sensitization pathways are also included [2, 4] in the mechanism development. The $NO_x$ chemistry is valid over not only high temperatures, but also over low-temperature and high-pressure conditions to account for the NO-hydrocarbon sensitization effect and $NO_x$ re-burn chemistry. The assembled $NO_x$ chemistry is based on several previous studies [14, 25, 26] and was reported in our earlier publications [2, 4].

Another important aspect of the detailed mechanism is the inclusion of thermodynamic and transport data for all the species. Thermodynamic data are generally estimated based on the group additivity method [27]; in some cases they are based

on high-level ab initio calculations, where available. We have updated thermodynamic data for several important species in the core combustion mechanism, based on recent findings [11-13, 28]. Representative species with updated thermodynamic data are shown in Table 1. Unlike in the original mechanism, all the elementary reactions in the RD2010 mechanism are written as reversible and the reverse-rate constants are calculated based on thermodynamics to assure microscopic reversibility of the system. The transport parameters, obtained from GRI-mech 3.0 [14], are similar to the original CHEMKIN parameters from Sandia National Laboratories [29]. Transport parameters are important for all flame simulations and for models where diffusion effects are important in addition to kinetics.

**Table 1. Updated thermodynamic parameters used in the RD2010 mechanism. Dot "•" represents a radical site. Units are kcal/mol for heats of formation, and cal/mol-K for entropy and heat capacities.**

| Species | $H_f$ 298K | S 298K | $C_P$ 298K | $C_P$ 2000K |
|---|---|---|---|---|
| $CH_2O$ | -25.93 | 52.3 | 8.5 | 18.1 |
| $CH_3O•$ | 3.96 | 55.9 | 9.5 | 23.1 |
| $C•H_2OH$ | -2.90 | 58.8 | 11.8 | 22.4 |
| $CH_3OC•O$ | -39.37 | 68.9 | 14.7 | 33.9 |
| $•OCHO$ | -41.24 | 57.9 | 9.8 | 19.1 |
| $HOCH_2O$ | -42.16 | 66.1 | 13.0 | 27.8 |
| $C_2H_3•$ | 71.64 | 55.9 | 10.2 | 23.3 |
| $CH_3CHO$ | -40.78 | 63.1 | 13.2 | 33.2 |
| $CH_3C•O$ | -3.38 | 64.3 | 12.4 | 28.1 |
| $HOC_2H_4CHO$ | -80.31 | 83.38 | 22.37 | 43.41 |

## 3. MODELING AND VALIDATION

Validation of the RD2010 core mechanism was performed using fundamental experimental data. Such experiments allow probing of kinetics effects and are less affected by heat-loss and turbulence-related effects. The data used in this study are from the combustion literature, published over the last four decades from 1971 to 2010. Table 2 shows the type of experimental data used for various fuels. The CHEMKIN-PRO [30] simulation package was employed for modeling each of the experiments. All the comparisons presented in this section show predictions from the RD2010 mechanism (represented by lines). The results shown here represent a selection of all available data, since it is not feasible to use all the data that has ever been published. However, we have selected the data such that a broad range of conditions are represented over the domain of available data. This way the model is shown to be valid for a large domain of fuels, experiments, and conditions that are pertinent to the combustion environments of most practical applications.

Fundamental experiments considered in this work include laminar flame speeds and ignition-delay times; these represent global characteristics of a combustion system. Flame extinction strain rate data were also used for hydrogen. In addition, we also considered many detailed species profiles from flow reactors, stirred reactors, and burner-stabilized flames. Simulations of stirred reactors provide good tests of kinetics with no transport effects, whereas flames also test the coupling of kinetics with transport. Together, the broad range of data selected provides a stringent test of the mechanism. Table 3 shows the range of conditions covered by various types of fundamental experiments. Lastly, we also validated the $NO_x$ submechanism using high-pressure burner-stabilized flames of methane. Comparisons of the predictions to the experimental data are discussed next for each fuel. It may be noted that only the most representative of the validation cases performed are shown in this paper, for brevity.

**Table 2. Coverage matrix for validation of the core mechanism.**

| Neat fuels | Laminar flame speed | Shock tube | Flow reactor | Stirred reactors |
|---|---|---|---|---|
| Hydrogen* | ✓ | ✓ | | |
| Formaldehyde | | | ✓ | |
| Methane | ✓ | ✓ | | |
| Methanol | | | | ✓ |
| Ethane | | ✓ | | |
| DME | ✓ | ✓ | ✓ | |
| Ethanol | ✓ | | | |
| Propane | ✓ | | | |
| *n*-Butane | ✓ | ✓ | | |
| *iso*-Butane | | ✓ | | |
| *n*-Butanol | ✓ | ✓ | | ✓ |

* Flame extinction data also used for validation
† Burner-stabilized flames used to validate the $NO_x$ submechanism.

**Table 3. Range of conditions covered by the data used for validation.**

| Experiment type | T (K) | P (atm) | ϕ | Dilution of oxidizer %* |
|---|---|---|---|---|
| **Laminar flame speed** | 295 to 453 | 1 to 5 | 0.6 to 1.6 | 0 to 15 |
| **Shock-tube** | 650 to 1800 | 1 to 340 | Pyrolysis, 0.3 to 3 | 0 to >98 |
| **Flow reactor** | 500 to 948 | 1.5 to 12.5 | 0.005 to 1.19 | 97.6 to 98.8 |
| **Stirred reactors** | 700 to 1100 | 10 | 0.6 to 1 | 97.1 to 97.9 |
| **Burner-stabilized flames†** | 300 | 1 to 14.6 | 0.6 to 0.8 | $N_2/O_2$ : 2.2/1 for oxidizer |

* Additional dilution with $N_2$, Ar, or $H_2O$ with air or $O_2$ as oxidizer.
† Used to validate $NO_x$ sub-mechanism using methane.

### 3.1 Hydrogen

Comparison of hydrogen laminar flame speeds at 298 K and 1 atm with air and $Ar/O_2$ oxidants are shown in Figure 1. Data from several sources are shown to illustrate the measurement scatter. All the reported data included for comparison have been extrapolated to zero stretch. Flame speeds with argon are higher and the model accurately captures all trends.

Comparisons were also performed for extinction strain rates for laminar hydrogen-air flames at 298 K and 1 atm. Data are from experiments performed by Egolfopoulos and co-workers [31, 32]. Predictions are in excellent agreement with their recent data [32]. Scatter in the data also shows possible uncertainty involved in measurements but we expect the more recent data to be more accurate.

Recently Herzler et al. [33] measured the autoignition-delay time of hydrogen using a dilute mixture of oxygen in argon at stoichiometric conditions and at various pressures from 1 to 16 atm. The data show interesting trends in ignition time at the different pressures. At temperatures below 1100 K, ignition times increase rapidly as pressure is increased. As seen in Figure 3, the model accurately captures all of these trends in hydrogen autoignition times.

### 3.2 Formaldehyde

Li et al. [11] measured the time evolution of species in the oxidation of formaldehyde at very lean and dilute conditions at several pressures, using $H_2O$ and $N_2$ for dilution. The temperature in their flow reactor stayed constant due to high levels of dilution. Figure 4 shows the comparison of predicted profiles of formaldehyde and CO at 1.5 atm and 948 K. Since the start of oxidation in the reactor is uncertain, as discussed by Li et al. [11], the experimental data are shifted by 0.12 s. Predictions are in excellent agreement with the data. Predictions for other pressures are also in good agreement but their plots are not included for brevity.

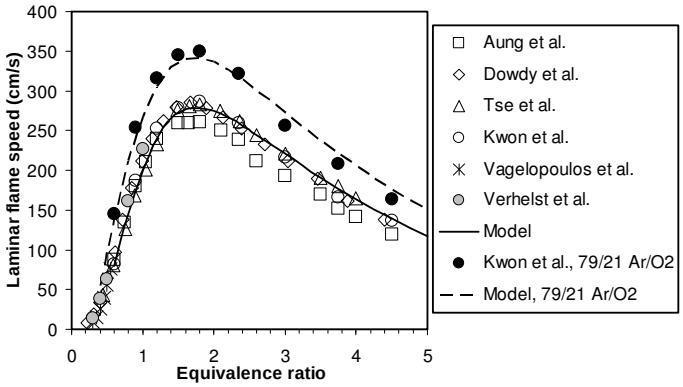


**Figure 1. Comparison of predicted hydrogen/air and hydrogen-$O_2$-Ar flame speeds at 1 atm and 298 K, with the experimental data of Dowdy et al. [34], Kwon et al. [35], Aung et al. [36], Tse et al. [37], Vagelopoulos et al. [38] and Verhelst et al. [39].**

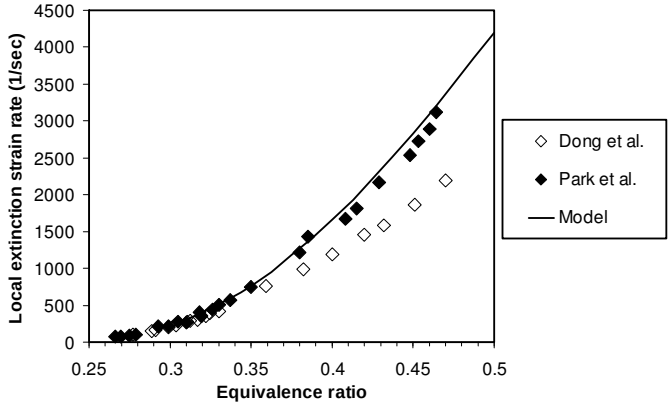


**Figure 2. Comparison of predicted hydrogen/air extinction strain rates at 1 atm and 298 K, with the experimental data of Dong et al. [31] and the recent data from Park et al. [32].**

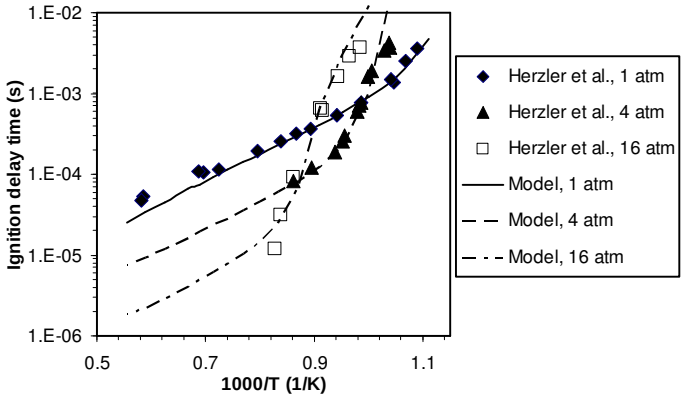


**Figure 3. Effect of pressure on ignition-delay times for stoichiometric hydrogen-oxygen-argon mixtures (91.2 mol% argon). Calculated values are compared with the experimental data of Herzler et al. [33].**

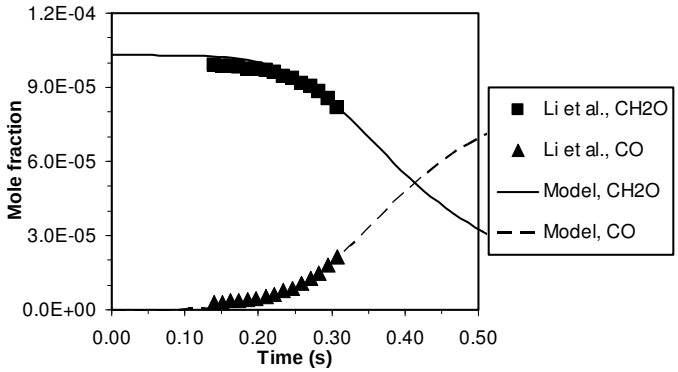


**Figure 4. Calculated profiles of $CH_2O$ and CO compared with the experimental data of Li et al. [11] during oxidation in a flow reactor at 948 K and 1.5 atm pressure using a mixture of $CH_2O/O_2/H_2O$:0.0103/2/0.37 mol% in $N_2$.**

### 3.3 Methane

Several researchers have measured laminar flame speeds of methane-air at 1 atm and 298 K. A comparison of predicted laminar flame speeds of methane-air to those measured by two different sources are shown in Figure 5. The typical uncertainty in the experimental data is approximately ±3 cm/s with higher uncertainty expected on the fuel-rich side, as discussed by Ji et al. [40]. Considering the uncertainties involved, predictions are in excellent agreement with the data.

Recently Petersen et al. [41, 42] measured the ignition time of methane-air mixtures at high pressures using a shock tube. They also measured ignition time for various equivalence ratios from 1 to 3. Figure 6 compared the predicted ignition times to those measured for a fuel-rich mixture at an equivalence ratio of 3 and pressures ranging from 40 to 140 atm. Predictions agree well with the data. Extended predictions to lower temperatures show the effect of negative temperature coefficient (NTC) behavior typically observed for larger hydrocarbons and related to their cool-flame behavior.

### 3.4 Methanol

Dayma et al. [45] measured species profiles for methanol oxidation in a stirred reactor at 10 atm over 700 to 1000 K. They used dilute fuel-lean mixtures with 8000 ppm of methanol with 800 ppm of water in oxygen-nitrogen mixtures with a residence time of 1 s. Comparisons of predicted species profiles in methanol oxidation for an equivalence ratio of 0.6 at 10 atm to those measured are shown in Figure 7. As seen in the figure, CO levels increase from 800 to 900 K and then slowly drops at higher temperatures. Formaldehyde is also a significant intermediate product. The model accurately captures all the species profiles.

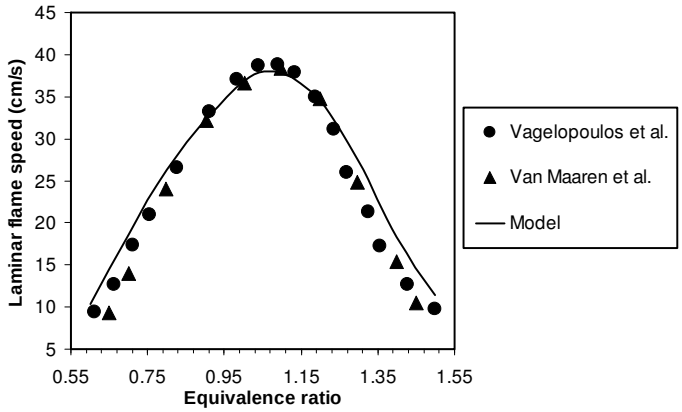


**Figure 5. Calculated flame speeds of methane-air mixtures at 1 atm and 298 K, compared with the data of Vagelopoulos et al. [43] and Van Maaren et al. [44].**

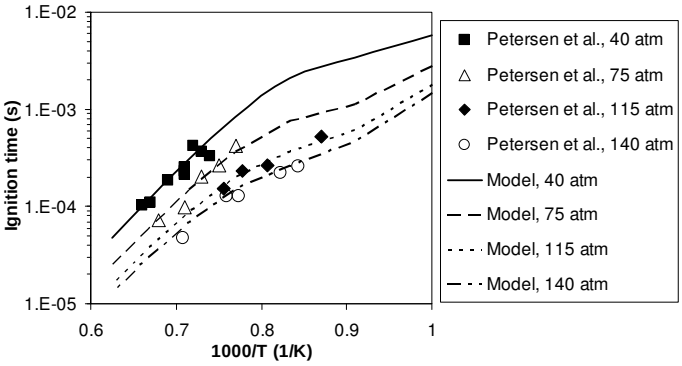


**Figure 6. Effect of pressure on ignition-delay times for a methane-oxygen-nitrogen mixture (20 mol% methane) with equivalence ratio of 3. Calculated values are compared with the experimental data of Petersen et al. [41] (data extracted from another Petersen reference [42]).**

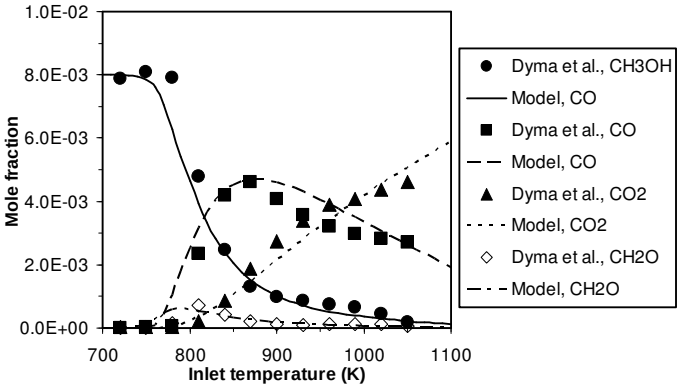


**Figure 7. Calculated methanol species profiles for oxidation conditions of a methanol-oxygen-nitrogen mixture, compared with the experimental data of Dayma et al. [45]. Conditions include 10 atm, inlet temperatures of 700-1100 K, and an equivalence ratio of 0.6. The inlet species included 8000 ppm of $CH_3OH$, 20,000 ppm of $O_2$ and 800 ppm of $H_2O$.**

### 3.5 Ethanol

Several groups measured laminar flame speeds of ethanol-air mixtures at various initial temperatures at 1 atm. Comparison of predicted flame speeds to those measured at 298 K, 360 K, and 453 K are shown in Figure 8. The scatter in the data from different experiments seems to be greater than that usually seen for non-oxygenated hydrocarbons. For example, at 360 K, the data near the peak at an equivalence ratio of 1.2 varies from 58 to 66 cm/s. In any case, the model predictions are within these uncertainties and the model accurately captures the effect of temperature and equivalence ratio on flame speeds for ethanol.

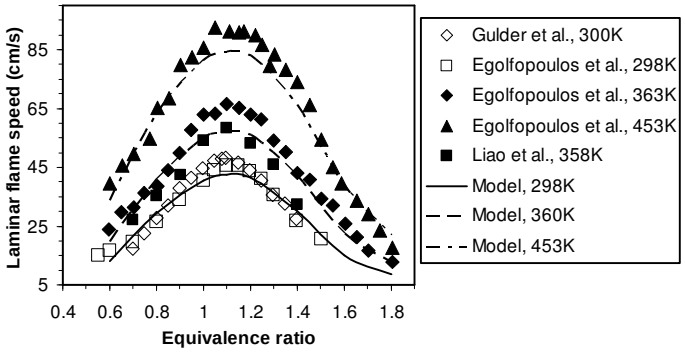


**Figure 8. Calculated flame speeds of ethanol-air mixtures at 1 atm, compared with the data of Egolfopoulos et al. [46], Gulder et al. [47], and Liao et al. [48] at various temperatures.**

### 3.6 Dimethyl ether (DME)

Several researchers measured laminar flame speeds of dimethyl ether (DME) mixed with air at 295 K and 1 atm. Similar to the observation for ethanol; the scatter in the data for DME is also higher than that observed for non-oxygenated hydrocarbons. Near the peak, flame-speed data vary from 45 to 53 cm/s. There are particularly large discrepancies under fuel-rich conditions. Despite the uncertainty, a clear trend in predictions can be seen in Figure 9 that is in good agreement with the data of Qin et al. [49], which fall in the middle of the other data.

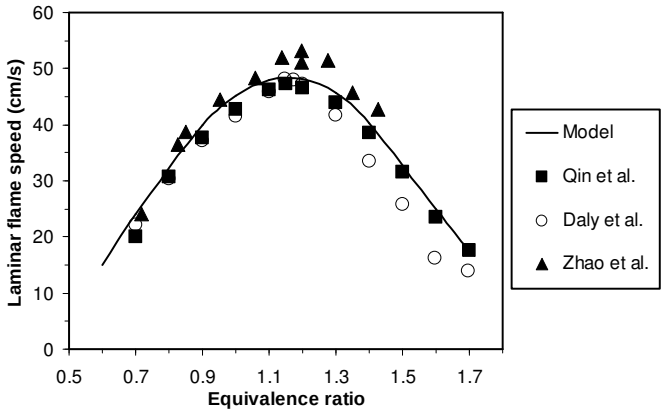


**Figure 9. Calculated flame speeds of dimethyl ether (DME)-air mixtures at 1 atm and 295 K, compared with the data of Qin et al. [49], Daly et al. [50], and Zhao et al. [51].**

Curran et al. [52] measured species during oxidation of DME in a flow reactor at different temperatures. The conditions used in the experiments were 3030 ppm of fuel in the mixture of oxygen-nitrogen at an equivalence ratio of 1.19. The operating pressure of the flow reactor was 12.5 atm and residence time was 1.8 s. Comparisons of predicted DME, CO, and $CO_2$ with those measured by Curran et al. are shown in Figure 10. The model accurately captures the slow down in reactivity as temperature is increased from 600 K to 700 K, as well as production of CO and $CO_2$.

Pfahl et al. [53] measured autoignition-delay time of stoichiometric DME-air mixtures in a shock tube at 13 bar and 40 bar pressures. As seen in Figure 11, the model clearly captures the NTC behavior in DME at both pressures.

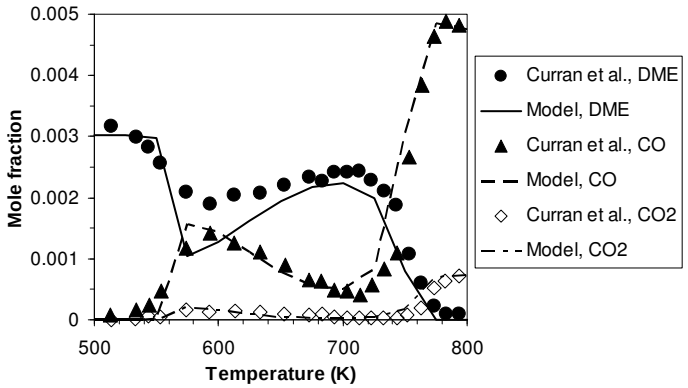


**Figure 10. Comparison of predicted species temporal profiles with those measured for oxidation of 3030 ppm DME in oxygen-nitrogen mixture, compared with the flow-reactor experimental data of Curran et al. [52] at 12.5 atm and equivalence ratio of 1.19.**

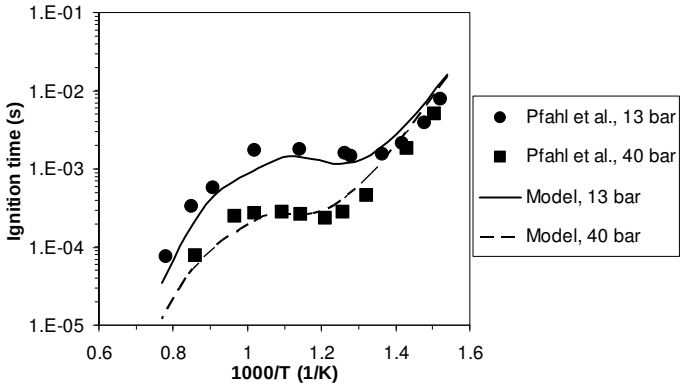


**Figure 11. Comparison of predicted autoignition times for a stoichiometric DME-air mixture at different pressures with those measured in a shock-tube by Pfahl et al. [53]**

## 3.7 Ethane

Laminar flame speeds for ethane-air have been measured by several researchers [54, 55] at 298 K and various pressures. As seen in Figure 12, predicted laminar flame speeds are in excellent agreement with the data at 1, 2, and 5 atm.

For ethane pyrolysis, predicted evolution of species vs. temperature under high-pressure shock-tube measurements seem to be shifted by ~20 K towards high temperatures, as seen in Figure 13. However, the predictions are still within the scatter of the data.

Predicted autoignition times for ethane are shown in Figure 14. These results show good agreement with the shock-tube data of Burcat et al. [56] at 10 atm and stoichiometric conditions.

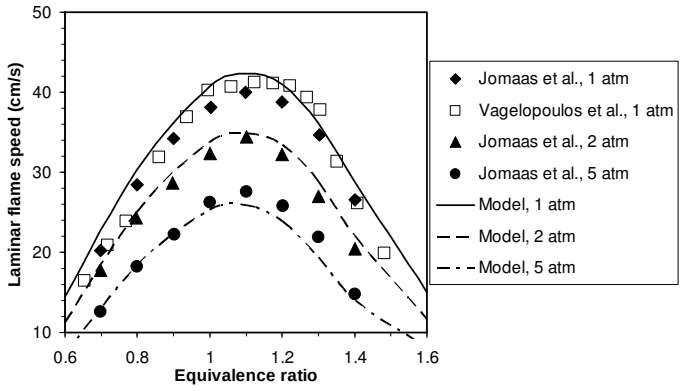


**Figure 12. Calculated flame speeds of ethane-air mixtures at 298 K and at various pressures of 1, 2 and 5 atm, compared with the data of Jomaas et al. [54] and Vagelopoulos et al. [55].**

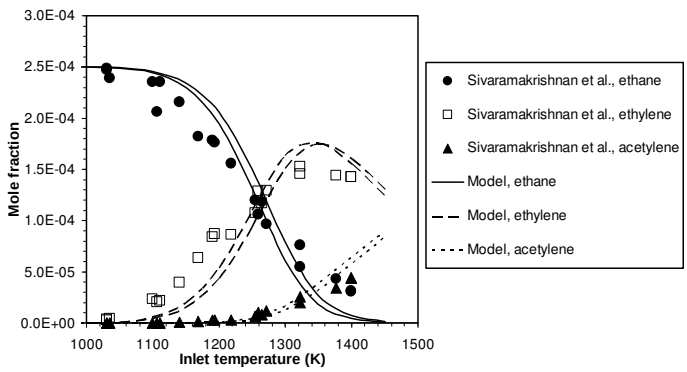


**Figure 13. Calculated $C_2H_6$, $C_2H_4$ and $C_2H_2$ species profiles for ethane pyrolysis (250 ppm ethane in argon), compared with the experimental data of Tranter et al. [57], at 340 bar. Two lines represent predictions with residence times of 1.25 and 1.6 ms due to uncertainty in the measurement.**

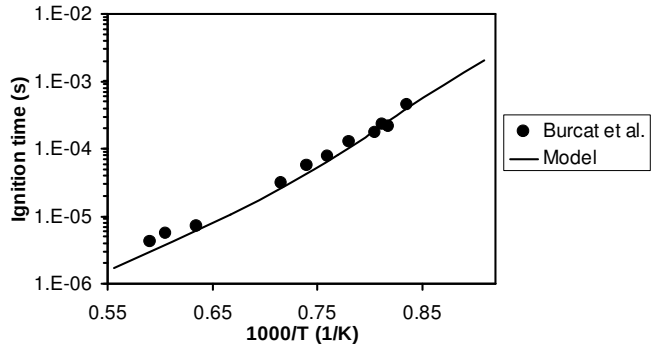


**Figure 14. Ignition times at 10 atm for stoichiometric ethane-$O_2$-Ar. Calculated values are compared with the experimental data of Burcat et al. [56].**

## 3.8 Propane

Figure 15 compares the calculated flame-speed values with the experimental data of Jomaas et al. [54] and Vagelopoulos et al. [55] at 298 K and pressures of 1, 2, and 5 atm. The predictions agree well with the data. The model also accurately captures the pressure effects within the uncertainty range of the data.

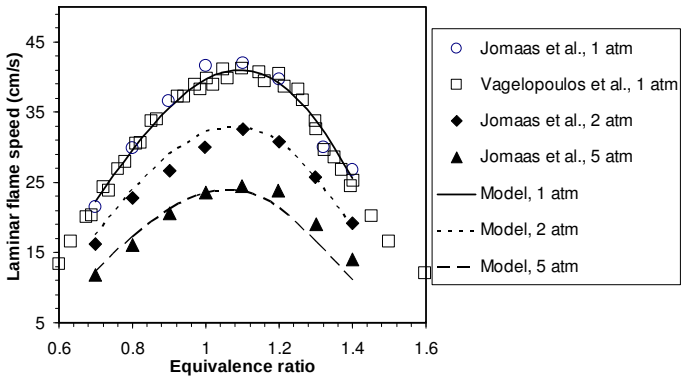


**Figure 15. Calculated flame speeds of propane-air mixtures at 298 K and at pressures of 1, 2, and 5 atm, compared with the data of Jomaas et al. [54] and Vagelopoulos et al. [55].**

### 3.9 *n*-Butane

Figure 16 compares the predicted flame speeds of *n*-butane at 1 atm and 298 K to those measured by Davis et al. [58]. The model predictions agree well with the data and are well within the uncertainty ranges of the data.

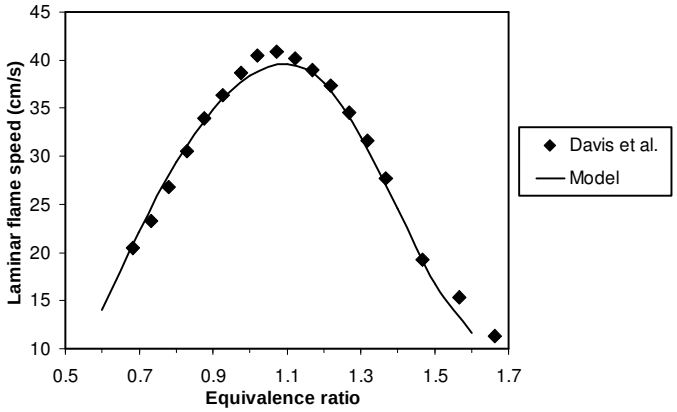


**Figure 16. Comparison of predicted flame speeds of *n*-butane-air with the experimental data of Davis et al. [58] at 1 atm and 298 K.**

Healy et al. [59] measured ignition times for a stoichiometric *n*-butane/$O_2$ mixture, with 81.25 mol% Ar dilution at 8 atm. The predictions shown in Figure 17 agree well with their experimental data. Healy et al. [59] also measured the ignition-delay times of *n*-butane/air mixtures over a range of equivalence ratios, pressures and temperatures. Figure 18 shows the effect of varying equivalence ratios, for a constant pressure of ~20 atm. The model is able to capture all of these effects. Though the RD2010 mechanism shows slightly slower ignition points at lower temperatures for fuel-lean conditions, they are within the expected uncertainties for fuel-air shock-tube experiments with ignition times above 1 ms.

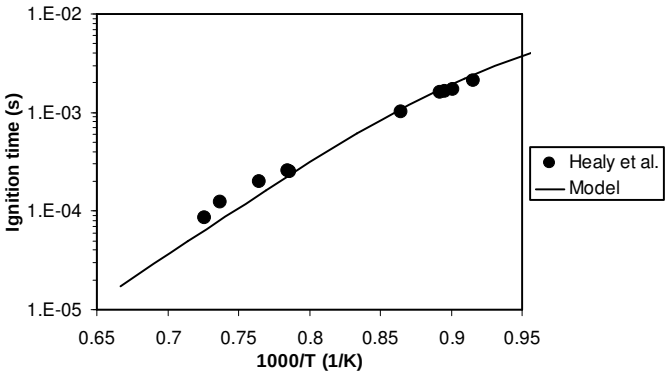


**Figure 17. Comparison of predicted ignition-delay times of a stoichiometric *n*-butane/$O_2$ mixture, and 81.25 mol% Ar dilution, at 8 atm with those measured by Healy et al. [59]**

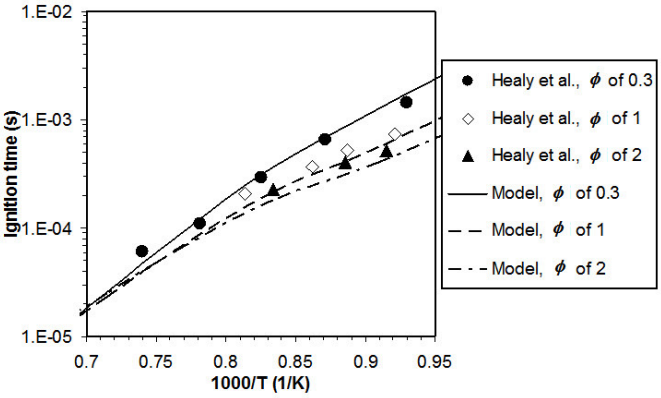


**Figure 18. Effect of changing equivalence ratio ($\phi$) on ignition-delay times of *n*-butane/air mixtures at a constant pressure of 20 atm. The data of Healy et al. [59] are compared with the model predictions.**

### 3.10 *iso*-Butane

Healy et al. [60] studied *iso*-butane/air ignition-delay times over equivalence ratios of 0.3-2, pressures of ~1-35 atm and temperatures of ~1100-1500 K. Figure 19 to Figure 21 show the predictions compared with the experimental data, for equivalence ratios of 0.3, 1, and 2. Predictions using the current mechanism are in excellent agreement with the data and capture the effect of temperature, pressure, and equivalence ratio.

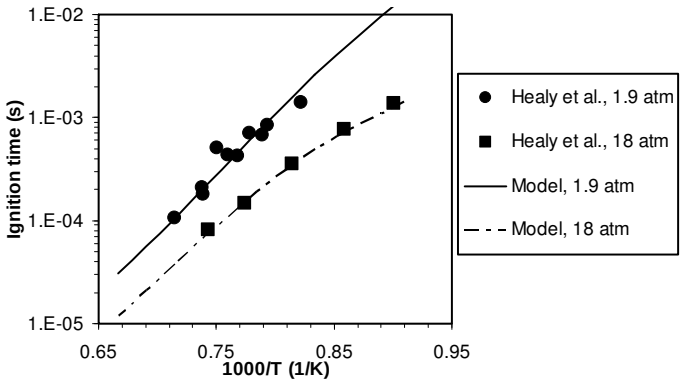


**Figure 19. Effect of changing pressures on ignition-delay times of *iso*-butane/air mixtures at a constant equivalence ratio of 0.3. The data of Healy et al. [59] are compared with the model predictions.**

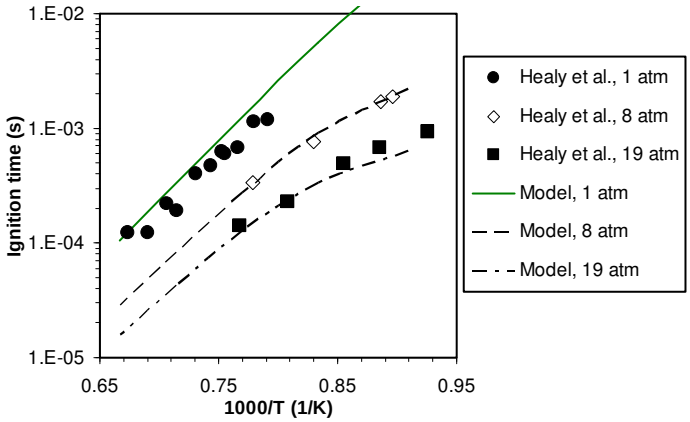


**Figure 20. Effect of changing pressures on ignition-delay times of stoichiometric mixture of *iso*-butane/air. The data of Healy et al. [59] are compared with the model predictions.**

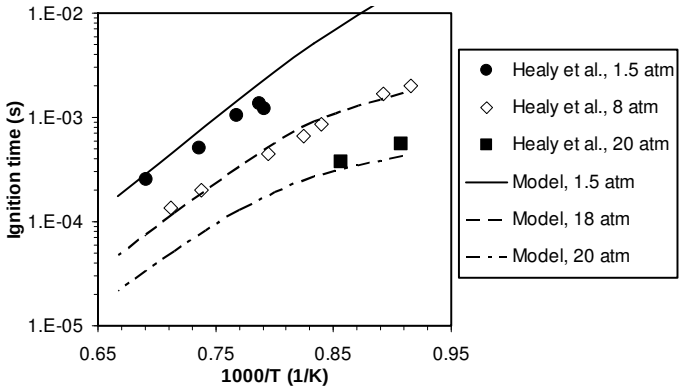


**Figure 21. Ignition-delay times of Healy et al. [60] compared with model predictions, for *iso*-butane/air mixtures. Pressures of 1.5, 8 and 20 atm were studied, for a constant equivalence ratio of 2.**

### 3.11 *n*-Butanol

Recently, Veloo et al. [61] measured the laminar flame speeds of *n*-butanol using a counter-flow burner assembly. They extrapolated to zero stretch using a non-linear extrapolation technique. A comparison of predicted flame speeds of *n*-butanol-air at elevated temperatures of 343 K and 1 atm to those measured by Veloo et al. [61] is shown in Figure 22. Predictions agree well with the data within measurement uncertainty limits.

Comparisons of predicted autoignition time for *n*-butanol/$O_2$/Ar mixtures to those measured by Moss et al. [62] using a shock tube are shown in Figure 23 to Figure 24. The model captures the trends with respect to changes in equivalence ratios and fuel loading at 1.2 atm.

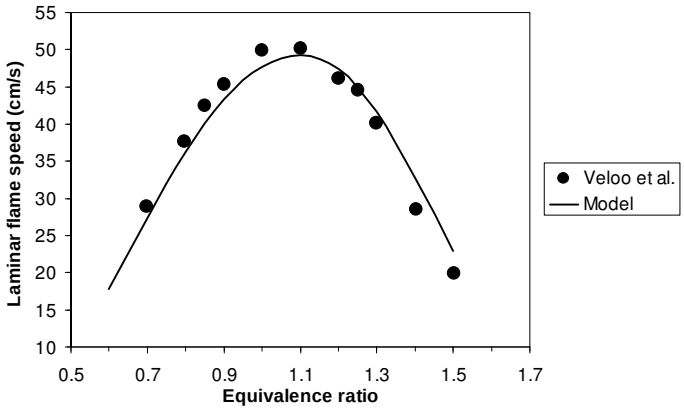


**Figure 22. Calculated flame speeds of *n*-butanol-air mixtures at 1 atm and 343 K, compared with the data of Veloo et al. [61].**

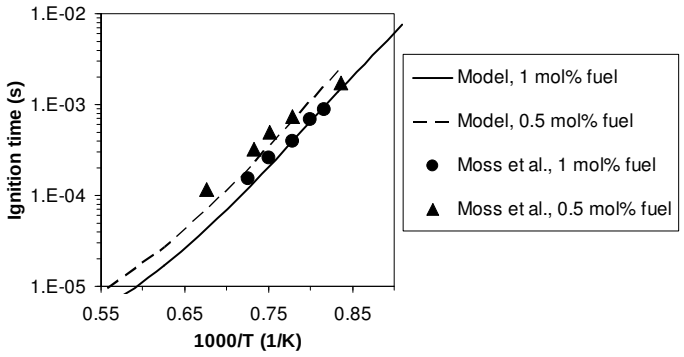


**Figure 23. Comparison of predicted autoignition time with that measured by Moss et al. [62] for *n*-butanol-$O_2$-Ar mixtures in a shock tube at equivalence ratio of 0.25 and nominal pressure of 1 atm.**

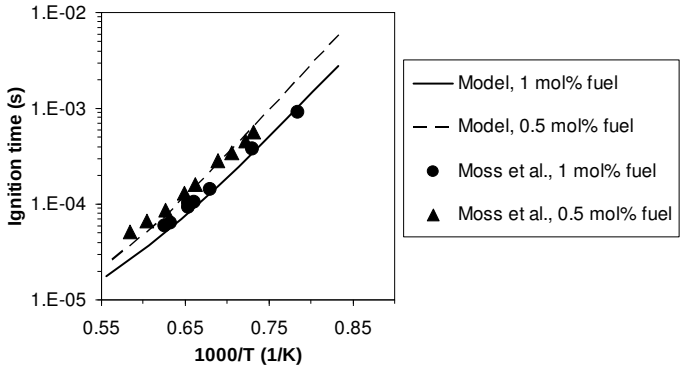


**Figure 24. Comparison of predicted autoignition time with that measured by Moss et al. [62] for *n*-butanol-$O_2$-Ar mixtures in a shock tube at stoichiometric conditions and nominal pressure of 1 atm.**

Black et al. [63] recently measured ignition time for *n*-butanol/$O_2$/Ar mixtures at slightly different conditions than those used by Moss et al. [62] using a shock tube. Black et al. measured ignition times at 2.6 and 8 atm, and 0.6 and 3.5 mol% fuel loading at various equivalence ratios. Figure 25 shows the effect of fuel loading on *n*-butanol ignition at 2.6 atm and stoichiometric conditions. Predictions agree well with the data. Figure 26 compares the predicted ignition time of *n*-butanol at various equivalence ratios at 0.6 mol% fuel and 8 atm. Predictions for stoichiometric and fuel-lean conditions agree well with the data.

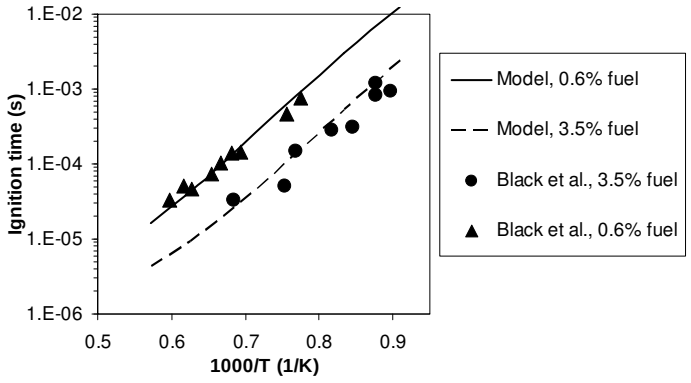


**Figure 25. Comparison of predicted autoignition time to that measured by Black et al. [63] for *n*-butanol-$O_2$-Ar mixtures in a shock tube at equivalence ratio of 1 and nominal pressure of 2.6 atm.**

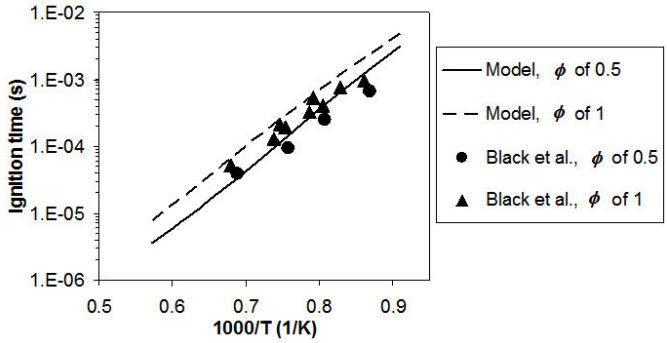


**Figure 26. Effect of equivalence ratio ($\phi$) on autoignition times of *n*-butanol-$O_2$-Ar mixture with 0.6% fuel at nominal pressure of 8 atm. The data of Black et al. [63] are compared with the model predictions.**

Dagaut et al. [64] measured species profiles in a stirred reactor for stoichiometric *n*-butanol/$O_2$/$N_2$ mixture with 1 mol% fuel at 10 atm and 0.7 s residence time. Comparisons between model and experiment for important product species are shown in Figure 27 and Figure 28. Trends with respect to the change in temperature are captured well. Predicted profiles of hydrogen and several $C_1$ species, including formaldehyde, agree well with the measurements. Profiles of *n*-butanol, butene (mostly 1-butene), and propene are captured well by the model. Profiles of $C_2$ species including ethylene, ethane, acetaldehyde, are all captured well.

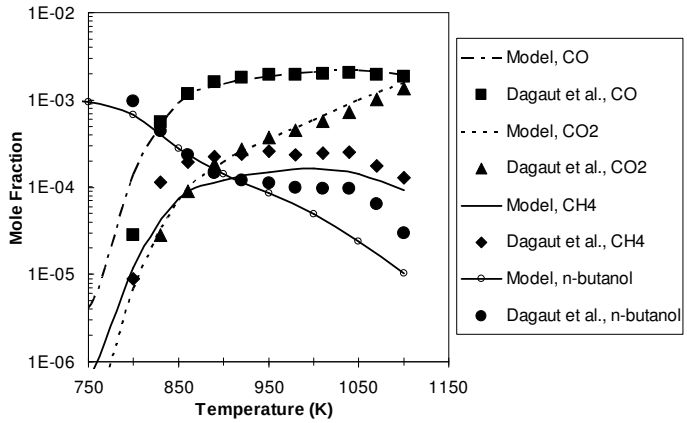


**Figure 27. Comparison of predicted species profiles to that measured by Dagaut et al. [64] for oxidation of 1 mol% *n*-butanol in $O_2$ and $N_2$ in a stirred reactor at equivalence ratio of 1.0, 10 atm, and residence time of 0.7 s. Closed symbols are experimental data and lines with open symbols are predictions.**

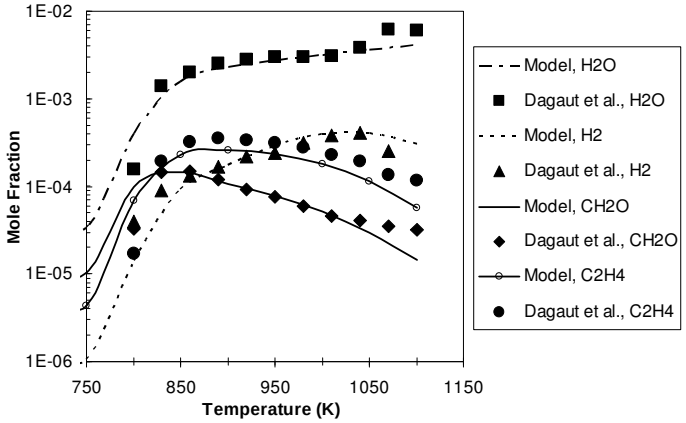


**Figure 28. Comparison of predicted species profiles to that measured by Dagaut et al. [64] for oxidation of 1 mol% *n*-butanol in $O_2$ and $N_2$ in a stirred reactor at equivalence ratio of 1.0, 10 atm, and residence time of 0.7 s. Closed symbols are experimental data and lines with open symbols are predictions.**

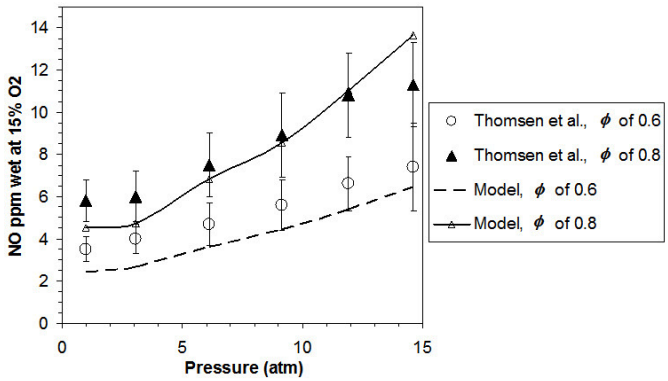


**Figure 29. Comparison of predicted effect of pressure on NO levels in methane-oxygen-nitrogen burner-stabilized flames at unburned mixture temperature of 300 K at various equivalence ratios ($\phi$) to those measured by Thomsen et al. [66] Oxidizer used is rich in oxygen with nitrogen/oxygen ratio of 2.2/1. CHEMKIN-PRO simulation includes the effect of radiation.**

### 3.12 $NO_x$

The comprehensive detailed reaction mechanism developed for core combustion chemistry also includes a $NO_x$ submechanism valid from low temperatures to high temperatures. $NO_x$ generation is a high-temperature phenomenon, but at low temperatures $NO_x$ reacts with hydrocarbons, resulting in mutual sensitization of the NO-hydrocarbon oxidation processes [25]. We reported validation of the $NO_x$ submechanism used in our previous publications [4, 65] for fuels that include smaller hydrocarbons and for liquid fuels. In this work, we have performed additional validation using high-pressure burner-stabilized flames of methane with an oxygen-rich oxidizer with nitrogen-oxygen ratio of 2.1-1 at the unburned mixture temperature of 300 K. In the CHEMKIN-PRO flame simulation, we also included radiation heat losses that lead to accurate prediction of temperatures. $NO_x$ measurements were taken at the height of 3 mm above the burner for pressures as high as 14.6 atm by Thomsen et al. [66]. A comparison of predicted-to-measured NO at 15% $O_2$ levels vs. pressure is shown in Figure 29. Predictions accurately capture the effect of pressure and equivalence ratio, even for low levels of NO below 20 ppm. With this validation we expect that predictions of NO formation for other fuels also should be accurate.

## 4. DISCUSSION

Significant progress has been made in improving the core mechanism for the targeted saturated components. Although the sheer number of cases used for validation makes it impractical to present analysis here of the mechanism for each case presented in this work, we performed analysis under selected conditions to get a diverse sampling of the details that are characteristic of the mechanism. The discussion includes reactions important to most flame-speed and autoignition-time predictions. The most sensitive reactions in the system that affect most $C_0$-$C_4$ saturated fuels are listed in Table 4. Reaction path analyses for oxidation of an oxygenated fuel at low temperatures have also been outlined.

A sensitivity analysis of flame speeds has been performed for pure fuels at 298 K, 1 atm, close to the peak-flame-speed equivalence ratio of 1.1. Figure 30 shows the analysis for $C_1$-$C_4$ saturated hydrocarbons. The four most important reactions (Rxn 1 to Rxn 4 in Table 4) are identical for all hydrocarbons and include reactions of the base $C_0$-$C_1$ chemistry. Reactions of $C_2$ and $C_3$ also appear in Figure 30. Of the four top-most important reactions, the rate constant for Rxn 2 has been increased by a factor of 1.24, which is well within the uncertainty level for this reaction. Any adjustments made to the rate constant were well within the uncertainty ranges derived from reaction-specific studies or from the NIST database [24]. The improved mechanism's accurate predictions of all flame speeds are a result of the core chemistry now being well characterized.

**Table 4. Important reactions and the source of their rate constants used in the mechanism. Rate coefficients are in units of cal, mol, cm³, K. Rate constants are calculated as $k = A*T^n*Exp(-Ea/RT)$ where $T$ represents temperature and $R$ represents the gas constant.**

| No. | Reaction | *A* | *n* | *Ea* | Ref. |
|---|---|---|---|---|---|
| 1 | $H+O_2 = O+OH$ | 3.55E+15 | -0.406 | 1.66E+04 | [12] |
| 2† | $CO+OH = CO_2+H$ | 2.20E+05 | 1.89 | -1.16E+03 | [12], A*1.24 |
| 3 | $HCO+M = H+CO+M$ | 4.75E+11 | 0.7 | 1.49E+04 | [11][a] |
| 4 | $H+OH+M = H_2O+M$ | 4.50E+22 | -2 | 0.00E+00 | [19][a] |
| 5 | $C_3H_5$-a+H(+M) = $C_3H_6$(+M) | 2.00E+14 | 0 | 0.00E+00 | [13] |
| | Low pressure limit: | 1.33E+60 | -12 | 5.97E+03 | |
| | Troe parameters: 0.02, 1.10E+03, 1.10E+03, 6.86E+03 | | | | |
| 6 | $CH_3+CH_3(+M) = C_2H_6(+M)$ | 9.21E+16 | -1.17 | 6.36E+02 | [12][a] |
| | Low pressure limit: | 1.14E+36 | -5.246 | 1.71E+03 | |
| | Troe parameters: 0.405, 1.12E+03, 69.6, 1.00E+10 | | | | |
| 7 | $CH_3+HO_2 = CH_3O+OH$ | 1.00E+12 | 0.269 | -6.88E+02 | [12] |
| 8 | $CH_4+H = CH_3+H_2$ | 6.14E+05 | 2.5 | 9.59E+03 | [12] |
| 9 | $HO_2+HO_2 = H_2O_2+O_2$ | 4.20E+14 | 0 | 1.20E+04 | [18][b] |
| | | 1.30E+11 | 0 | -1.63E+03 | |
| 10 | $CH_4+HO_2 = CH_3+H_2O_2$ | 1.13E+01 | 3.74 | 2.10E+04 | [12] |
| 11 | $CH_3O_2+CH_3 = CH_3O+CH_3O$ | 5.08E+12 | 0 | -1.41E+03 | [12] |
| 12 | $CH_3+OH = CH_2(S)+H_2O$ | 4.51E+17 | -1.34 | 1.42E+03 | [12] |
| 13 | $CH_3+O_2 = CH_2O+OH$ | 2.64E+00 | 3.283 | 8.11E+03 | [12] |
| 14 | $CH_3+H(+M) = CH_4(+M)$ | 2.14E+15 | -0.4 | 0.00E+00 | [6][a] |
| | Low pressure limit: | 3.31E+30 | -4 | 2.11E+03 | |
| | Troe parameters: 0.0, 1.00E-15, 1.00E-15, 40.0 | | | | |
| 15† | $C_2H_4+H(+M) = C_2H_5(+M)$ | 1.95E+12 | 0.454 | 1.82E+03 | [12][a], A*1.8 |
| | Low pressure limit: | 2.16E+42 | -7.62 | 6.97E+03 | |
| | Troe parameters: 0.975, 210., 984., 4.37E+03 | | | | |

[a] Collision efficiencies: $CH_4$ 2.0, CO 1.9, $CO_2$ 3.8, $C_2H_6$ 3.0, $H_2O$ 6.0, $H_2$ 2.0, Ar 0.7

[b] Rate constant is the sum of two expressions.

† c.f. text.

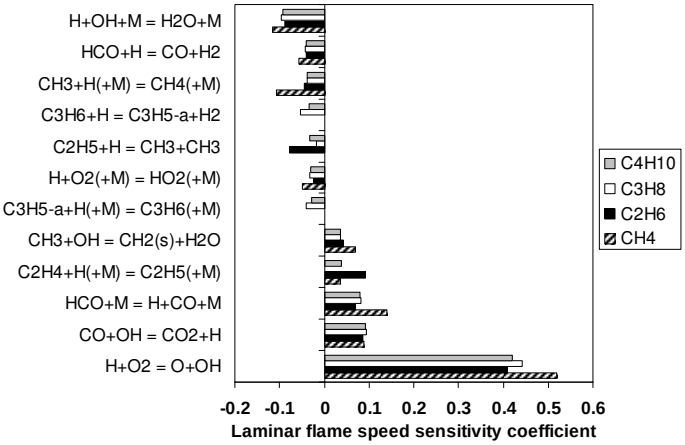


**Figure 30. Sensitivity analysis of laminar flame speed at 298K, 1 atm, and equivalence ratio of 1.1 for various saturated core components.**

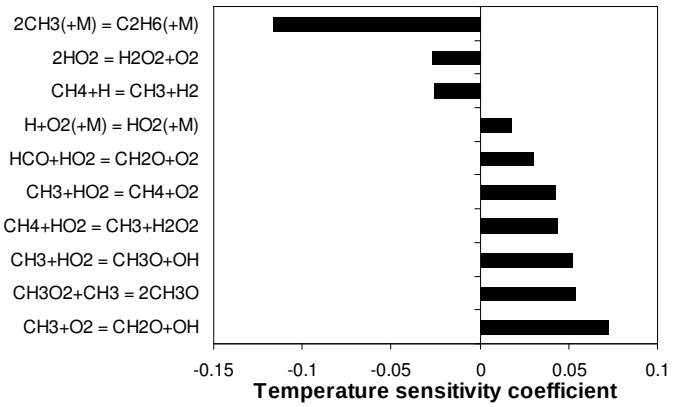


**Figure 31. Temperature sensitivity analysis for methane-air autoignition under shock-tube conditions of Petersen et al. [41] at equivalence ratio of 3, 140 atm, 1400 K, and 10% conversion.**

Temperature sensitivity analyses have been performed for autoignition experiments for methane at the high-pressure and fuel-rich conditions described in Figure 6. As shown in Figure 31, many reactions identified in the sensitivity analyses, such as Rxn 6, Rxn 7, Rxn 8, etc., from Table 4 are also sensitive to flame speeds for many fuels, as found in Figure 30. Rate constants for all of these important reactions have been taken from published sources without any adjustments, as described in Table 4. One striking aspect of the analysis here is that, at very fuel-rich conditions, methane autoignition is not sensitive to the chain-branching Rxn 1 from Table 4; however, reactions of $RO_2$ and $HO_2$ become more important at such high pressures. Rxn 9 to Rxn 15 from Table 4 are also the most important reactions based on the sensitivity analyses of both flame speeds and autoignition-time simulations. Rate constants for ethyl radical dissociation, Rxn 15, have been increased by a factor of 1.8. For

this pressure-dependent reaction the expected uncertainty is not less than a factor of 2.

Reaction path analysis for DME has been performed for autoignition experiments in a shock-tube [53], as reported in Figure 11. Figure 32 shows the flux diagram for an initial temperature and pressure of 850 K and 40 atm, and at 20% fuel conversion. DME exhibits two-stage ignition similar to that observed in larger alkanes, such as *n*-heptane [6], and the first-stage ignition results in 20% fuel conversion with temperature increased to 1000 K. Low-temperature kinetics involving $O_2$ addition to the parent radical and subsequent chemistry [6] dominates the process. Major intermediate species produced are $H_2O_2$, $CH_3OOH$, and CO, and the chemistry is governed by the reactions involving OH and $HO_2$ radicals, as seen in Figure 32. As temperature increases further, peroxide species dissociate to produce more reactive OH radicals that eventually lead to autoignition. As seen in the path diagram, formaldehyde is the major species during the entire oxidation process of DME. In this way, the kinetics of formaldehyde significantly affects DME too. The comprehensive reaction mechanism developed in this work successfully captures such interdependencies of the combustion kinetics for the large number of fuel species considered.

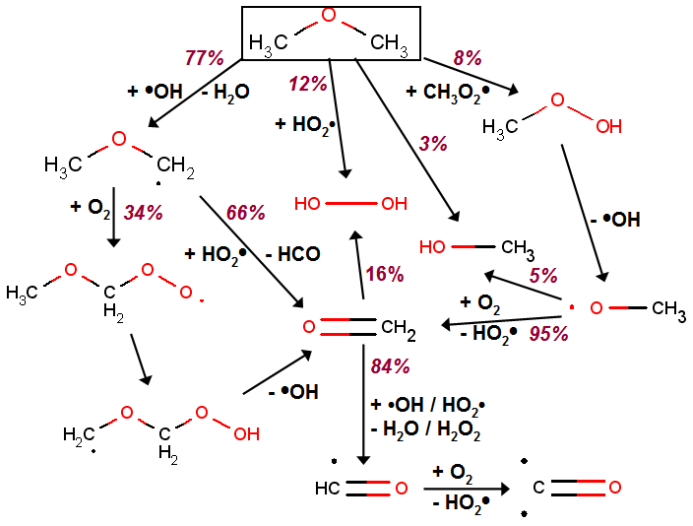


**Figure 32. Reaction path diagram for dimethyl ether under the shock-tube conditions of Pfahl et al. [53], as shown in Figure 11. The initial conditions included temperature of 850 K, pressure of 40 atm, equivalence ratio of 1.0, and the reaction path diagram is at 20% fuel conversion. Branching ratios are shown in percentage.**

## 5. CONCLUSIONS

A careful study of the $C_0$-$C_4$ core chemistry has been undertaken to address known issues in model predictions that are common to many published hydrocarbon mechanisms. In this work, we took a systematic approach to improve the core kinetics that are shared with larger hydrocarbon fuel components. We have validated the new self-consistent mechanism containing chemistry of all core components against fundamental experiments that cover a range of saturated fuel components, experimental conditions, and types of experiments. The new mechanism reported here shows excellent agreement with data, well within the experimental uncertainties evident for each study. The mechanism development was achieved primarily by adding missing reaction paths, improving thermodynamic data, and considering uncertainties in reaction-rate data for key reactions.


## Acknowledgement

This work has been supported in part by the Model Fuels Consortium II (www.modelfuelsconsortium.com).


## 6. REFERENCES


1. Puduppakkam, K.V., Naik, C.V., and Meeks, E. *Validation Studies of a Master Kinetic Mechanism for Diesel and Gasoline Surrogate Fuels*. in *SAE World Congress*. 2010.
2. Naik, C.V., Puduppakkam, K.V., Modak, A., et al., *Validated F-T Fuel Surrogate Model For Simulation of Jet-Engine Combustion.* Proc. ASME Turbo Expo, 2010. **GT2010-23709**.
3. Naik, C.V., Puduppakkam, K.V., and Meeks, E., *Applying Detailed Kinetics to Realistic Engine Simulation: the Surrogate Blend Optimizer and Mechanism Reduction Strategies.* SAE Int. J. Engines, 2010. **3**(1): p. 241-259.
4. Naik, C.V., Puduppakkam, K.V., and Meeks, E., *Modeling the Detailed Chemical Kinetics of Mutual Sensitization in the Oxidation of a Model fuel for Gasoline and Nitric Oxide* SAE Int. J. Fuels Lubr., 2010. **3**(1): p. 556-566.
5. Puduppakkam, K., Liang, L., Naik, C.V., et al., *Combustion and Emissions Modeling of an HCCI Engine Using Model Fuels.* SAE Technical Papers, 2009. **2009-01-0669**.
6. Westbrook, C.K., Pitz, W., Herbinet, O., et al., *A Detailed Chemical Kinetic Reaction Mechanism for Combustion of n-Alkanes from n-Octane to n-Hexadecane.* Comb. Flame, 2009. **156**: p. 181-191.
7. Curran, H.J., Gaffuri, P., Pitz, W.J., et al., *A Comprehensive Modeling Study of Iso-Octane Oxidation.* Comb. Flame, 2002. **129**: p. 253-280.
8. Naik, C.V., Pitz, W.J., Sjöberg, M., et al., *Detailed Chemical Kinetic Modeling of Surrogate Fuels for Gasoline and Application to an HCCI Engine.* SAE Technical Papers, 2005. **2005-01-3741**.
9. Pitz, W.J., Naik, C.V., Mhaoldúin, T.N., et al., *Modeling and Experimental Investigation of Methylcyclohexane*

*Ignition in a Rapid Compression Machine.* Proc. Comb. Inst., 2007. **31**: p. 267.
10. Naik, C.V. and Dean, A.M., *Modeling High Pressure Ethane Oxidation and Pyrolysis.* Proc. Comb. Inst., 2009. **32**(1): p. 437-443.
11. Li, J., Zhao, Z., Kazakov, A., et al., *A Comprehensive Kinetic Mechanism for CO, CH2O, and CH3OH Combustion.* Int. J. Chem. Kinet., 2007. **39**: p. 109-136.
12. Healy, D., Kalitan, D.M., Aul, C.J., et al., *Oxidation of C1−C5 Alkane Quinternary Natural Gas Mixtures at High Pressures.* Energy & Fuels, 2010. **24**(3): p. 1521-1528.
13. A high-temperature chemical kinetic model of n-alkane oxidation, JetSurF version 1.0 http://melchior.usc.edu/JetSurF/Index.html: 2009.
14. Smith, G.P., Golden, D.M., Frenklach, M., et al. *GRI-Mech 3.0*. [cited; Available from: http://www.me.berkeley.edu/gri_mech/.
15. Naik, C.V., Puduppakkam, K.V., and Meeks, E., *An Improved Core Reaction Mechanism for Un-saturated $C_0$-$C_4$ Fuels and their Blends.* In preparation, 2011.
16. Curran, H.J., Gaffuri, P., Pitz, W.J., et al., *A Comprehensive Modeling Study of n-Heptane Oxidation.* Comb. Flame, 1998. **114**: p. 149-177.
17. Naik, C.V., Westbrook, C.K., Herbinet, O., et al., *Detailed Chemical Kinetic Reaction Mechanism for Biodiesel Components Methyl Stearate and Methyl Oleate.* Proc. Comb. Inst., 2010. **33**: p. doi:10.1016/j.proci.2010.05.007.
18. Konnov, A.A., *Remaining uncertainties in the kinetic mechanism of hydrogen combustion.* Comb. Flame, 2008. **152**: p. 507-528.
19. O'Conaire, M., Curran, H.J., Simmie, J.M., et al., *A Comprehensive Modeling Study of Hydrogen Oxidation.* Int. J. Chem. Kinet., 2004. **36**: p. 603-622.
20. Healy, D., Kopp, M.M., Polley, N.L., et al., *Methane/n-Butane Ignition Delay Measurements at High Pressure and Detailed Chemical Kinetic Simulations.* Energy Fuels, 2010. **24**: p. 1617–1627.
21. Laskin, A., Wang, H., and Law, C.K., *Detailed Kinetic Modeling of 1,3-Butadiene Oxidation at High Temperatures.* Int. J. Chem. Kinet., 2000. **May 16, 2000**: p. 589-614.
22. Zhang, H.R., Eddings, E.G., Sarofim, A.F., et al., *Fuel Dependence of Benzene Pathways.* Proc. Comb. Inst., 2009. **32**: p. 377-385.
23. Troe, J., *Approximate Expressions for the Yields of Unimolecular Reactions with Chemical and Photochemical Activation.* J. Phys. Chem., 1983. **87**(10): p. 1800 - 1804.
24. NIST Chemical Kinetics Database, Standard Reference Database 17 7.0 (Web Version),
25. Rasmussen, C.L., Rasmussen, A.E., and Glarborg, P., *Sensitizing Effects of NOx on CH4 Oxidation at High Pressure.* Comb. Flame, 2008. **154**(3): p. 529-545.
26. Dagaut, P., Glarborg, P., and Alzueta, M.U., *The Oxidation of Hydrogen Cyanide and Related Chemistry.* Prog. Energy Combust. Sci., 2008. **34**: p. 1-46.
27. Ritter, E.R., *THERM: a computer code for estimating thermodynamic properties for species important to combustion and reaction modeling.* Journal of Chemical Information and Computer Sciences, 1991. **31**(3): p. 400-408.
28. NIST Standard Reference Database 69, 2010.
29. Chemkin Collection Release 3.6, Reaction Design, Inc.: San Diego, CA, 2000.
30. CHEMKIN-PRO 15101, Reaction Design: San Diego, 2010.
31. Dong, Y., Holley, A.T., Andac, M.G., et al., *Extinction of premixed H2/air flames: Chemical kinetics and molecular diffusion effects.* Comb. Flame, 2005. **142**: p. 374-387.
32. Park, O., Veloo, P.S., Liu, N., et al., *Combustion Characteristics of Alternative Gaseous Fuels.* Proc. Comb. Inst., 2010. **33**.
33. Herzler, J. and Naumann, C., *Shock-tube study of the ignition of methane/ethane/hydrogen mixtures with hydrogen contents from 0% to 100% at different pressures.* Proc. Comb. Inst., 2009. **32**: p. 213-220.
34. Dowdy, D.R., Smith, D.B., Taylor, S.C., et al., *The use of expanding spherical flames to determine burning velocities and stretch effects in hydrogen/air mixtures.* Twenty-Third Symposium (International) on Combustion, 1990. **23** p. 325–332.
35. Kwon, O.C. and Faeth, G.M., *Flame/Stretch Interactions of Premixed Hydrogen-Fueled Flames: Measurements and Predictions.* Combustion and Flame, 2001. **124**: p. 590–610.
36. Aung, K.T., Hassan, M.I., and Faeth, G.M., *Flame stretch interactions of laminar premixed hydrogen/air flames at normal temperature and pressure.* Combustion and Flame, 1997. **109**: p. 1-24.
37. Tse, S.D., Zhu, D.L., and Law, C.K., *Morphology and burning rates of expanding spherical flames in H2/O2/inert mixtures up to 60 atmospheres.* Proceedings of the Combustion Institute, 2000. **28**: p. 1793–1800.
38. Vagelopoulos, C.M. and Egolfopoulos, F.N., *Laminar Flame Speeds and Extinction Strain Rate of Mixtures of Carbon Monoxide with Hydrogen, Methane, and Air.* Proc. Comb. Inst., 1994. **25**: p. 1317-1323.
39. Verhelst, S., Woolley, R., Lawes, M., et al., *Laminar and unstable burning velocities and Markstein lengths of hydrogen–air mixtures at engine-like conditions.* Proceedings of the Combustion Institute 2005. **30**: p. 209–216.
40. Ji, C., Dames, E., Wang, Y.L., et al., *Propagation and Extinction of Premixed $C_5$-$C_{12}$ n-Alkane Flames.* Comb. Flame, 2009. **157**: p. 277-287.
41. Petersen, E.L., Davidson, D.F., and Hanson, R.K., *Kinetics Modeling of Shock-Induced Ignition in Low-Dilution*

*CH4/O2 Mixtures at High Pressures and Intermediate Temperatures.* Comb. Flame, 1999. **117**: p. 272-290.
42. Petersen, E.L., Kalitan, D.M., Simmons, S., et al., *Methane/Propane Oxidation at High Pressures: Experimental and Detailed Chemical Kinetic Modeling.* Proc. Comb. Inst., 2007. **31**: p. 447-454.
43. Vagelopoulos, C.M., Egolfopoulos, F.N., and Law, C.K., *Further Considerations on the Determination of Laminar Flame Speeds with the Counterflow Twin-Flame Technique.* Proc. Comb. Inst., 1994. **25**: p. 1341
44. Van Maaren, A., Thung, D.S., and de Goey, L.P.H., *Measurement of flame temperature and adiabatic burning velocity of methane/air mixtures.* Combustion Science and Technology, 1994. **96**(4-6): p. 327-344.
45. Dayma, G., Ali, K.H., and Dagaut, P., *Experimental and detailed kinetic modeling study of the high pressure oxidation of methanol sensitized by nitric oxide and nitrogen dioxide.* Proceedings of the Combustion Institute 2007. **31** p. 411–418.
46. Egolfopoulos, F.N., Du, D.X., and Law, C.K. *A Study on Ethanol Oxidation Kinetics in Laminar Premixed Flames, Flow Reactors, and Shock Tubes*. in *Twenty-Fourth Symposium (International) on Combustion*. 1992. Pittsburgh, PA: Combustion Institute.
47. Gulder, O.L. *Laminar burning velocities of methanol, ethanol and isooctane-air mixtures*. in *Nineteenth Symposium (International) on Combustion*. 1982.
48. Liao, S.Y., Jiang, D.M., Huang, Z.H., et al., *Determination of the laminar burning velocities for mixtures of ethanol and air at elevated temperatures.* Applied Thermal Engineering, 2007: p. 374-380.
49. Qin, X. and Ju, Y., *Measurements of burning velocities of dimethyl ether and air premixed flames at elevated pressures.* Proceedings of the Combustion Institute, 2005. **30**: p. 233-240.
50. Daly, C.A., Simmie, J.M., Wurmel, J., et al., *Burning Velocities of Dimethyl Ether and Air.* Combustion and Flame, 2001. **125**: p. 1349-1340.
51. Zhao, Z., Chaos, M., Kazakov, A., et al., *Thermal Decomposition Reaction and a Comprehensive Kinetic Model of Dimethyl Ether.* Int. J. Chem. Kinet., 2008. **40**: p. 1-18.
52. Curran, H.J., Fischer, S.L., and Dryer, F.L., *The Reaction Kinetics of Dimethyl Ether. II: Low- Temperature Oxidation in Flow Reactors.* Int. J. Chem. Kinet., 2000. **32**: p. 741-759.
53. Pfahl, U., Fieweger, K., and Adomeit, G., *Self-ignition of diesel-relevant hydrocarbon-air mixtures under engine conditions.* Proc. Comb. Inst., 1996. **26**: p. 781-789.
54. Jomaas, G., Zheng, X.L., Zhu, D.L., et al., *Experimental Determination of Counterflow Ignition Temperatures and Laminar Flame Speeds of $C_2$–$C_3$ Hydrocarbons at Atmospheric and Elevated Pressures.* Proc. Comb. Inst., 2005. **30**: p. 193-200.
55. Vagelopoulos, C.M. and Egolfopoulos, F.N., *Direct experimental determination of laminar flame speeds.* Proc. Comb. Inst., 1998. **27**: p. 513.
56. Burcat, A., Scheller, K., and Lifshitz, A., *Shock-Tube Investigation of Comparative Ignition Delay Times for $C_1$-$C_5$ Alkanes.* Combust. Flame, 1971. **16**: p. 29-33.
57. Tranter, R.S., Raman, A., Sivaramakrishnan, R., et al., *Ethane Oxidation and Pyrolysis from 5 Bar to 1000 Bar: Experiments and Simulation.* 2005.
58. Davis, S.G. and Law, C.K., *Determination of and fuel structure effects on laminar flame speeds of C1 to C8 hydrocarbons.* Comb. Sci. Technol., 1998. **140**: p. 427-449.
59. Healy, D., Donato, N.S., Aul, C.J., et al., *n-Butane: Ignition delay measurements at high pressure and detailed chemical kinetic simulations.* Combustion and Flame, 2010. **157**: p. 1526–1539.
60. Healy, D., Donato, N.S., Aul, C.J., et al., *Isobutane ignition delay time measurements at high pressure and detailed chemical kinetic simulations.* Combustion and Flame, 2010. **157** p. 1540–1551.
61. Veloo, P.S., Wang, Y.L., Egolfopoulos, F.N., et al., *A Comparative Experimental and Computational Study of Methanol, Ethanol, and n-Butanol Flames.* Comb. Flame, 2010. **157**(10): p. 1989-2004.
62. Moss, J.T., Berkowitz, A.M., Oehlschlaeger, M.A., et al., *An Experimental and Kinetic Modeling Study of the Oxidation of the Four Isomers of Butanol.* J. Phys. Chem. A, 2008. **112**(43): p. 10843-10855.
63. Black, G., Curran, H.J., Pichon, S., et al., *Bio-butanol: Combustion properties and detailed chemical kinetic model.* Combustion and Flame, 2010. **157** p. 363–373.
64. Dagaut, P., Sarathy, S.M., and Thomson, M.J., *A chemical kinetic study of n-butanol oxidation at elevated pressure in a jet stirred reactor.* Proc. Comb. Inst., 2009. **32**: p. 229-237.
65. Naik, C.V., Puduppakkam, K.V., Modak, A., et al., *Detailed Chemical Kinetic Mechansim for Alternate Jet Fuel Surrogates.* Comb. Flame, 2010. **Article in press**(doi:10.1016/j.combustflame.2010.09.016).
66. Thomsen, D.D., Kuligowski, F.F., and Laurendeau, N.M., *Modeling of NO Formation in Premixed, High-Pressure Methane Flames.* Combust. Flame, 1999. **119**: p. 307 - 318.